Optics Letters

Observation of spatial optical diametric drive acceleration in photonic lattices

Yumiao Pei,[1] Yi Hu,[1,*] Cibo Lou,[2] Daohong Song,[1] Liqin Tang,[1] Jingjun Xu,[1,4] and Zhigang Chen[1,3,5]

[1]The MOE Key Laboratory of Weak-Light Nonlinear Photonics, TEDA Applied Physics Institute and School of Physics, Nankai University, Tianjin 300457, China
[2]Faculty of Science, Ningbo University, Ningbo 315211, China
[3]Department of Physics and Astronomy, San Francisco State University, San Francisco, California 94132, USA
[4]e-mail: jjxu@nankai.edu.cn
[5]e-mail: zhigang@sfsu.edu
*Corresponding author: yihu@nankai.edu.cn

We experimentally and theoretically demonstrate a spatial diametric drive acceleration of two mutually incoherent optical beams in 1D optical lattices under a self-defocusing nonlinearity. The two beams, exciting the modes at the top/bottom edges of the first Bloch band and hence experiencing normal/anomalous diffraction, can bind together and bend in the same direction during nonlinear propagation, analogous to the interplay between two objects with opposite signs of mass that breaks Newton's third law. Their spatial spectrum changes associated with the acceleration are analyzed for different lattice modulations. We find that the acceleration limit is determined by the beam exciting the top band edge that reaches a saturated momentum change prior to the other pairing beam. © 2017 Optical Society of America

Although negative mass is still a concept appearing mostly in theory, its associated dynamics is counterintuitive and fascinating [1–9]. In particular, as predicted from Newton's third law of motion, the interaction between two objects with opposite mass may lead to their locked acceleration in a diametric drive fashion [10], where the positive mass experiences an attracting force while the negative one experiences a repelling force. Realizing such a prediction was hampered due to the failure in searching negative mass. It might be possible, however, to study this interaction by using an electron of effective negative mass in crystals, where the effective mass of a Bloch state is defined from the second derivative of the energy band. Unfortunately, such diametric drive acceleration for electrons has never been realized. Attention turned to photonic analog that could demonstrate the interaction of optical states with positive and negative "mass." Analogous to the definition in condensed matter physics, the mass sign of an optical state in the temporal configuration can be switched by employing different types of dispersion relationship (analogous to that of the energy band for electrons). Typically, an optical pulse propagating in the anomalous (normal) dispersion region corresponds to a state of positive (negative) mass. Under the action of an optical Kerr nonlinearity, for instance, two pulses of different mass sign can be forced to accelerate synchronously [6,7].

In the spatial domain, diffraction can be engineered by using periodically arranged waveguide arrays, allowing coexistence of anomalous and normal diffractions [11]. The interplay of optical states locating in the same region of either type of diffraction has been investigated in a variety of scenarios, always showing the behavior of either attraction or repulsion [12,13]. Nevertheless, to the best of our knowledge, two light beams experiencing different diffraction types (i.e., of opposite mass signs) in such spatial optical structures have not been considered in terms of their interaction and propagation dynamics. They may exhibit a diametric drive acceleration under the effect of a nonlinearity that may offer new ways for light steering and control.

In this Letter, we demonstrate the nonlinear interaction of two mutually incoherent beams with opposite signs of effective "mass" in a one-dimensional optical waveguide array. Under proper initial conditions, the two beams are able to join forces and propagate along the same bending trajectory. Such a diametric drive experiment is performed in titanium-diffused waveguides in a LiNbO$_3$ crystal, where a self-defocusing nonlinearity offers the "forces" for the interaction. Our experimental results are corroborated with numerical simulations.

The cross-phase modulation of the two incoherent beams in 1D photonic lattices embedded in a LiNbO$_3$ crystal is governed by the normalized coupled nonlinear Schrödinger equations [14,15]

$$i\frac{\partial \psi_1}{\partial z} + \frac{\partial^2 \psi_1}{\partial x^2} + V(x)\psi_1 = \Gamma \frac{|\psi_1|^2 + |\psi_2|^2}{1 + (|\psi_1|^2 + |\psi_2|^2)}\psi_1, \quad \textbf{(1a)}$$

$$i\frac{\partial \psi_2}{\partial z} + \frac{\partial^2 \psi_2}{\partial x^2} + V(x)\psi_2 = \Gamma \frac{|\psi_1|^2 + |\psi_2|^2}{1 + (|\psi_1|^2 + |\psi_2|^2)}\psi_2, \quad \textbf{(1b)}$$

where x and z are the dimensionless transverse and longitudinal coordinates, respectively, and they are linked to the laboratory coordinates (X, Z) by $x = X/d$ and $z = Z/(2kd^2)$ (d is the lattice period and k is the wavenumber within the crystal); $\psi_{1,2}$ are the slowly varying envelopes of the two incident beams, $V(x) = 2kd^2 k_0 A \cos^2(\pi x)$ (where k_0 is the vacuum wavenumber and A is the lattice modulation depth) is the normalized periodic potential associated with the waveguide array, and Γ is the normalized nonlinear coefficient related to the photorefractive photovoltaic effect [14,15].

From the Bloch theorem, the translation symmetry can introduce Bloch transmission bands in the momentum space (propagation constant β versus transverse wave vector k_x) separated by the forbidden gaps [16]. Normal and anomalous diffraction relationships coexist in each band. Without loss of generality and for a more feasible experiment, the Bloch band consisting of fundamental modes is considered, as schematically plotted in the first Brillouin zone (BZ) in Fig. 1(a). The normal and anomalous diffraction regions are separated by a nondiffraction point. Two incoherent beams located in different diffraction regions can be employed for our study. As a typical example, two beams matching the Bloch modes at top (Γ point) and bottom (M point) band edges are employed and they are marked as Γ- and M- beams, respectively. In the linear regime, the two beams behave differently when they encounter a negative defect (an index change lower than the lattice modulation) embedded in the waveguide array. Γ-beam experiences a "reflection" when it meets the defect [Fig. 1(b)], similar to the beam dynamics in common homogeneous media as a light beam of normal diffraction tends to travel toward the high-index region due to Snell's law. By using the paraxial propagation equation $\partial \psi / \partial z = i D \partial^2 \psi / \partial x^2$ (where D is the diffraction coefficient), one can infer that the beam dynamics in normal and anomalous diffraction regions are conjugate to each other. Therefore, on the contrary, M-beam tends to be attracted by the low-index defect [Fig. 1(c)]. Under the action of a self-defocusing nonlinearity, either of them can induce a negative potential by itself. When they interact in the configuration with
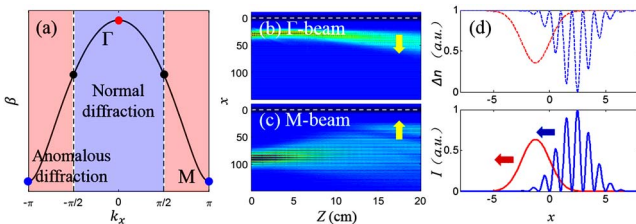
a beam-center mismatch as typically plotted in Fig. 1(d), Γ- and M-beams tend to move along the same transverse direction (here leftward) as a result of a repulsion and an attraction forces brought by each other. If the initial condition is elaborately chosen, the two beams are able to bind to accelerate together.

Our experimental setup is shown in Fig. 2. We use two different lasers to launch two mutually incoherent beams ($\lambda = 532$ nm) for granting the cross-phase modulation between them. Each beam, extraordinarily polarized and featured with a controllable amplitude modulation (a slit for Γ-beam and two parallel slits for M-beam), is sent to the Fourier plane of a $10\times$ objective lens by a 4-f system (not shown here), and then becomes a Gaussian or a cosine Gaussian beam at the front facet of the waveguide array, fabricated by titanium-diffusion in a copper-doped $LiNbO_3$ crystal that has a self-defocusing nonlinearity arising from the bulk photovoltaic effect [14,15]. The waveguide length is 14 mm and the array period d is 6.8 μm. The ratio between the peak intensities of the incident Γ-beam and M-beam is about $1.15 : 1$. The incident beam patterns are captured by CCD1, as shown in the inset of Fig. 2. The power and polarization of both beams are adjusted by employing a half-wave plate and a polarizer inserted in the 4-f system. The beam patterns at the output of the crystal and their spatial spectral components are recorded by CCD2 and CCD3, respectively.

In our experiment, the Gaussian beam and the cosine Gaussian beam, separated by a proper distance, are launched nearly at normal incidence into the lattice, and their spectral components are distributed around the center and the boundaries of the first BZ to excite the Bloch modes of Γ point and M point, respectively. First, their independent propagations are examined without considering the influence of each other. At a sufficiently low input power, both beams experience linear diffraction and their outputs are shown in Figs. 3(a) and 3(b). By employing a properly higher input power, Γ-beam becomes wider compared to the linear output [Fig. 3(c)], while M-beam evolves into a gap soliton as a result of the balance between the self-defocusing nonlinearity and the anomalous diffraction [Fig. 3(d)] [14,15]. The beam centers (obtained by calculating the "center of mass" of beams along X direction via $\int X dX \int I dY / \iint I dX dY$, where I is the beam intensity) of the nonlinear outputs almost coincide with that of the linear counterparts. Once the two beams are launched into the lattices simultaneously, the centers of both beams shift to the left under the interaction [Figs. 3(e) and 3(f)]. The shift for Γ-beam is not

Fig. 1. (a) Typical first Bloch band of 1D photonic lattice, where the normal and anomalous diffraction regions, separated by no-diffraction points (black), are shaded in blue and red, and top and bottom band edges are marked by Γ and M, respectively; (b) and (c) show numerically linear propagation of Γ-beam and M-beam in the lattice with an embedded negative defect (marked by a white-dashed line), and the yellow arrows point to lateral beam movement due to the presence of the defect; (d) negative refractive index changes (upper panel) induced by Γ-beam (red) and M-beam (blue) plotted in the bottom panel, where the arrows show the directions of transverse shifts of the two beams influenced by each other under a defocusing nonlinearity.
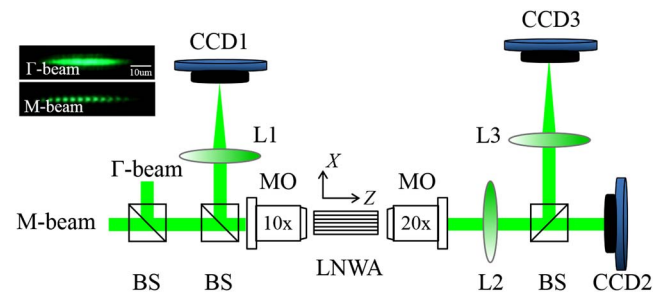
Fig. 2. Experiment setup. L1, L2, L3, convex lenses; BS, beam splitter; MO, microscope objective; LNWA, lithium niobate waveguide array. The insets are incident patterns of Γ- and M-beams recorded by CCD1.
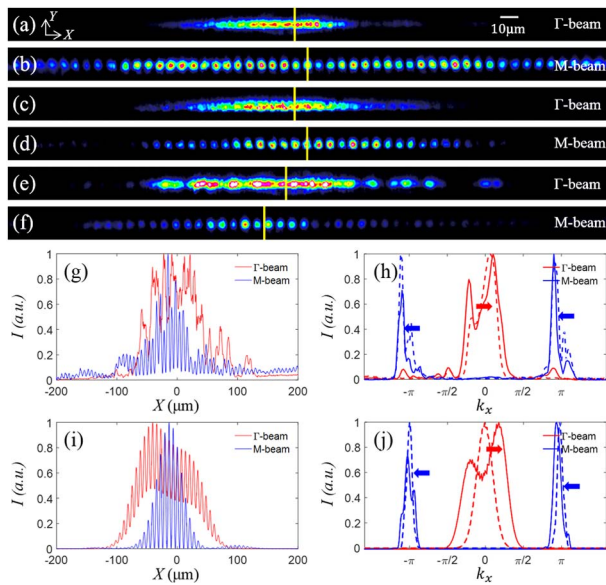
Fig. 3. Experimental results for a spatial diametric drive acceleration and the associated numerical simulations. (a, b) Linear and (c)–(f) nonlinear outputs for Γ-beam or M-beam propagating (a)–(d) independently or (e, f) under the cross-phase modulation. The vertical yellow lines indicate the location of the beam centers. (g) Plots of the intensity distribution obtained by integrating (e) and (f) along Y direction, and (h) their corresponding spectra (solid line). The dashed lines in (h) are the spectra for the linear output. (i) and (j) show results from numerical simulations corresponding to (g, h), respectively. The arrows in (h) and (j) show the shift directions of the spectra contributing to the diametric drive acceleration.

Fig. 4. Numerical simulations of the diametric drive acceleration extending the simulation in Fig. 3 in a propagation distance 4 times longer than the crystal length (marked by the yellow-dashed vertical lines). Upper and bottom rows show the side view of beam propagation and associated spectrum evolution of (a, c) Γ-beam or (b, d) M-beam that are numerically filtered out, where the black- and white-dashed horizontal lines mark the edge and nondiffraction region of the first BZ, respectively.

as obvious as that for M-beam. This is reasonable if one looks into the output beam profiles in detail shown in Fig. 3(g). Indeed, Γ-beam is separated into two parts due to the nonlinear interaction, and only the left part is repelled by M-beam. Therefore, the overall shift of Γ-beam becomes subtle as averaged by the right part. This is furthermore verified by the measurements in the Fourier space, where the spectrum for Γ-beam is accordingly divided into two components. Both parts move toward the higher-frequency side compared to the linear case, and hence the net momentum change for the whole Γ-beam does not become significant [Fig. 3(h)]. In contrast, all the spectral components for M-beam move in the same direction during the nonlinear interaction, indicating a larger movement of this beam in real space. Besides, these spectra at the boundary of the first BZ have an opposite (net) change as compared to those for Γ-beam, as a result of different diffraction types that the two beams experience. By using the parameters similar to those in the experiment, we numerically calculated the outputs and the associated spectra as presented in Figs. 3(i) and 3(j), and they agree well with the experimental results.

Furthermore, owing to the short propagation distance (14 mm as limited by the crystal length) in the experiment, the beam dynamics can be better visualized in Fig. 4 that extends the previous simulation to a longer distance. Here each beam is filtered out numerically to present in different panels. They show clearly a diametric drive acceleration, but only part of Γ-beam is bound with M-beam [Figs. 4(a) and 4(b)]. This is consistent with the analysis in Ref. [6], where the diametric
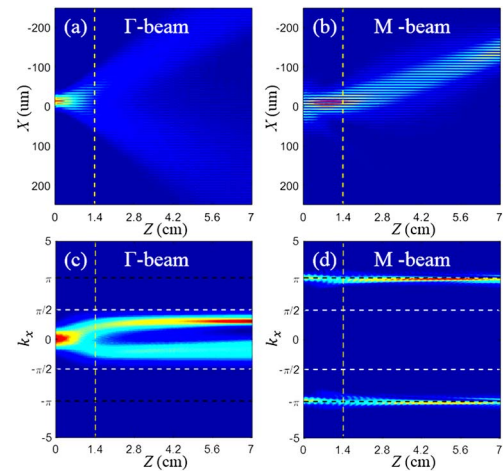
drive acceleration is formed by a soliton pursuing a dispersive wave. To obtain a shape-preserving bound state, the soliton is the one (of symmetrical shape) that can exist independently, but the dispersive wave should be carefully designed according to the soliton profile and eventually have an asymmetric shape. In our case, although Γ-beam (analogous to the dispersive wave) is carefully chosen in terms of power and width, its symmetrical pattern does not meet the requirement (asymmetry) of a perfect solution. Consequently, Γ-beam is dramatically shaped during the interaction. Although the beams contributing to the diametric drive move along the same path, the associated spectral change rate $\tau(z)$ (defined by the shift per unit propagation distance) for Γ-beam is much larger [Figs. 4(c) and 4(d)]. This difference originates from different curvatures of diffraction relationship. Under the paraxial condition described by Eq. (1), the diffraction is mainly determined by β'', which is -0.0946 (0.4373) for Γ (M) point in our waveguide lattice (the lattice modulation is $A = 5.0e - 4$). According to the definition of momentary velocity $v(z) = \beta'' \tau(z)$ [6], the spectrum of Γ-beam will thus attain a larger shift rate than that of M-beam. When the spectrum approaches the nondiffraction point where infinite mass is defined, the acceleration is gradually reduced and eventually becomes zero [7], analogous to that a relativistic particle cannot be accelerated to the vacuum speed of light as its mass tends to be infinite [17]. At this time, both beams stop acceleration, and their spectral shifts saturate accordingly. Since Γ-beam reaches this limit far prior to M-beam, it leads to the velocity saturation of this bound state. In addition, our preliminary numerical results show that the mutually coherent Γ-beam and M-beam can also lead to a diametric drive acceleration.

The diffraction curvature around the top/bottom band edges is likely to be altered by employing different lattice modulations. The calculated β'' for Γ and M points are plotted in Fig. 5(a) as a function of the lattice modulation A.
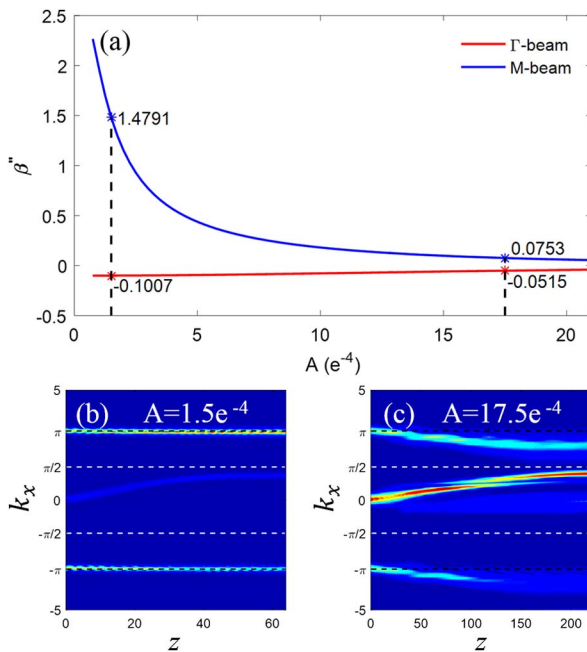
Fig. 5. (a) Second-order diffraction (β'') for band top (red line) and band bottom (blue line) calculated for different lattice modulation depth A; (b, c) show the spectrum evolution associated with diametric drive accelerations of Γ-beam and M-beam at lower ($A = 1.5e^{-4}$) and higher ($A = 17.5e^{-4}$) lattice modulation depth, where the black- and white-dashed lines mark the edge and the nondiffraction region of the first BZ, respectively.

incoherent optical beams in photonic lattices under a self-defocusing nonlinearity. It is found that, for the Bloch band consisting of fundamental modes, the acceleration limit is determined by the beam at the band top that always experiences diffraction of less strength under different lattice modulations. We expect that such a spatial diametric drive acceleration is possible in a nonlinear medium even without periodic structure by employing one beam with a nonlinearly induced negative mass [19]. Our results may bring about a new route for spatial light control by light, particularly when extending this approach into 2D (transverse) cases.

Their absolute values decrease when the lattice modulation is tuned up, and the one associated with M point changes drastically. In the lower depth modulation, since the band bottom is much more curved than the band top, the spectrum for M-beam is mostly located around the boundaries of the first BZ under the condition of diametric drive acceleration [Fig. 5(b)]. When the lattice modulation is quite large, the beam is tightly confined in a single waveguide and the well-known tight-binding model can be approximately employed. In this framework, the diffraction curve is described by a cosine function [18], leading to the same absolute curvature for the top and bottom band edges. This model is gradually approached as the lattice modulation is increased. Thus for a sufficiently high lattice modulation, M-beam can reach a lateral shift in the spectrum domain comparable to that of Γ-beam when they bound to accelerate [Fig. 5(c)]. Since the diffraction experienced by Γ-beam is always larger than M-beam, the acceleration saturation is only determined by Γ-beam.

In conclusion, we have experimentally and theoretically demonstrated the spatial diametric drive acceleration of two

REFERENCES

1. H. Bondi, Rev. Mod. Phys. **29**, 423 (1957).
2. R. T. Hammod, Eur. J. Phys. **36** (2015).
3. C. Luo, S. G. Johnson, J. D. Joannopoulos, and J. B. Pendry, Phys. Rev. B **65**, 201104 (2002).
4. H. Sakaguchi and B. A. Malomed, J. Phys. B **37**, 1443 (2004).
5. O. Morsch and M. Oberthaler, Rev. Mod. Phys. **78**, 179 (2006).
6. S. Batz and U. Peschel, Phys. Rev. Lett. **110**, 193901 (2013).
7. M. Wimmer, A. Regensburger, C. Bersch, M. A. Miri, S. Batz, G. Onishchukov, D. N. Christodoulides, and U. Peschel, Nat. Phys. **9**, 780 (2013).
8. M. A. Khamehchi, K. Hossain, M. E. Mossman, Y. Zhang, Th. Busch, M. M. Forbes, and P. Engels, Phys. Rev. Lett. **118**, 155301 (2017).
9. W. B. Bonnor and F. I. Cooperstock, Phys. Lett. A **139**, 442 (1989).
10. M. G. Millis, J. Propul. Power **13**, 577 (1997).
11. H. S. Eisenberg, Y. Silberberg, R. Morandotti, and J. S. Aitchison, Phys. Rev. Lett. **85**, 1863 (2000).
12. J. Meier, G. I. Stegeman, Y. Silberberg, R. Morandotti, and J. S. Aitchison, Phys. Rev. Lett. **93**, 093903 (2004).
13. S. Liu, Y. Hu, P. Zhang, X. Gan, F. Xiao, C. Lou, D. Song, J. Zhao, J. Xu, and Z. Chen, Opt. Lett. **36**, 1167 (2011).
14. F. Chen, M. Stepić, C. E. Rüter, D. Runde, D. Kip, V. Shandarov, O. Manela, and M. Segev, Opt. Express **13**, 4314 (2005).
15. E. Smirnov, M. Stepić, C. E. Rüter, D. Kip, and V. Shandarov, Opt. Lett. **31**, 2338 (2006).
16. D. Mandelik, H. S. Eisenberg, Y. Silberberg, R. Morandotti, and J. S. Aitchison, Phys. Rev. Lett. **90**, 053902 (2003).
17. M. Born, Ann. Phys. **335** (1909).
18. D. N. Christodoulides and R. I. Joseph, Opt. Lett. **13**, 794 (1988).
19. F. Di Mei, P. Caramazza, D. Pierangeli, G. Di Domenico, H. Ilan, A. J. Agranat, P. Di Porto, and E. DelRe, Phys. Rev. Lett. **116**, 153902 (2016).